Search for point sources of ultra-high-energy photons with the Telescope Array surface detector

R. U. Abbasi,[1] M. Abe,[2] T. Abu-Zayyad,[1] M. Allen,[1] R. Azuma,[3] E. Barcikowski,[1]
J. W. Belz,[1] D. R. Bergman,[1] S. A. Blake,[1] R. Cady,[1] B. G. Cheon,[4] J. Chiba,[5]
M. Chikawa,[6] A. di Matteo [7]†T. Fujii,[8,9] K. Fujita,[10] R. Fujiwara,[10]
M. Fukushima,[11,12] G. Furlich,[1] W. Hanlon,[1] M. Hayashi,[13] Y. Hayashi,[10]
N. Hayashida,[14] K. Hibino,[14] K. Honda,[15] D. Ikeda,[11] N. Inoue,[2] T. Ishii,[15]
R. Ishimori,[3] H. Ito,[16] D. Ivanov,[1] H. M. Jeong,[17] S. Jeong,[17] C. C. H. Jui,[1]
K. Kadota,[18] F. Kakimoto,[3] O. Kalashev,[19] K. Kasahara,[20] H. Kawai,[21] S. Kawakami,[10]
S. Kawana,[2] K. Kawata,[11] E. Kido,[11] H. B. Kim,[4] J. H. Kim,[1] J. H. Kim,[22]
S. Kishigami,[10] V. Kuzmin,[19]‡ M. Kuznetsov,[7,19]★ Y. J. Kwon,[23] K. H. Lee,[17]
B. Lubsandorzhiev,[19] J. P. Lundquist,[1] K. Machida,[15] K. Martens,[12] T. Matsuyama,[10]
J. N. Matthews,[1] R. Mayta,[10] M. Minamino,[10] K. Mukai,[15] I. Myers,[1] S. Nagataki,[16]
K. Nakai,[10] R. Nakamura,[24] T. Nakamura,[25] T. Nonaka,[11] H. Oda,[10] S. Ogio,[10,26]
M. Ohnishi,[11] H. Ohoka,[11] T. Okuda,[27] Y. Omura,[10] M. Ono,[16] R. Onogi,[10]
A. Oshima,[10] S. Ozawa,[20] I. H. Park,[17] M. S. Pshirkov,[19,28] J. Remington,[1] D.
C. Rodriguez,[1] G. Rubtsov,[19]★ D. Ryu [22] H. Sagawa,[11] R. Sahara,[10] K. Saito,[11]
Y. Saito,[24] N. Sakaki,[11] T. Sako,[11] N. Sakurai,[10] L. M. Scott,[29] T. Seki,[24] K. Sekino,[11]
P. D. Shah,[1] F. Shibata,[15] T. Shibata,[11] H. Shimodaira,[11] B. K. Shin,[10] H. S. Shin,[11]
J. D. Smith,[1] P. Sokolsky,[1] B. T. Stokes,[1] S. R. Stratton,[1,29] T. A. Stroman,[1] T. Suzawa,[2]
Y. Takagi,[10] Y. Takahashi,[10] M. Takamura,[5] M. Takeda,[11] R. Takeishi,[17] A. Taketa,[30]
M. Takita,[11] Y. Tameda,[31] H. Tanaka,[10] K. Tanaka,[32] M. Tanaka,[33] Y. Tanoue,[10] S.
B. Thomas,[1] G. B. Thomson,[1] P. Tinyakov,[7,19] I. Tkachev,[19] H. Tokuno,[3] T. Tomida,[24]
S. Troitsky [19] Y. Tsunesada,[10,26] K. Tsutsumi,[3] Y. Uchihori,[34] S. Udo,[14] F. Urban,[35]
T. Wong,[1] K. Yada,[11] M. Yamamoto,[24] H. Yamaoka,[33] K. Yamazaki,[14] J. Yang,[36]
K. Yashiro,[5] H. Yoshii,[37] Y. Zhezher,[19] and Z. Zundel[1] (Telescope Array Collaboration)

Affiliations are listed at the end of the paper

ABSTRACT

The surface detector (SD) of the Telescope Array (TA) experiment allows us to detect indirectly photons with energies of the order of 10^{18} eV and higher, and to separate photons from the cosmic ray background. In this paper, we present the results of a blind search for point sources of ultra-high-energy (UHE) photons in the Northern sky using the TA SD data. The photon-induced extensive air showers are separated from the hadron-induced extensive air shower

---

★ E-mail: mkuzn@inr.ac.ru (MK); grisha@ms2.inr.ac.ru (GR)
† Now at INFN, sezione di Torino, Turin, Italy
‡ Deceased

background by means of a multivariate classifier based upon 16 parameters that characterize the air shower events. No significant evidence for the photon point sources is found. The upper limits are set on the flux of photons from each particular direction in the sky within the TA field of view, according to the experiment's angular resolution for photons. The average 95 per cent confidence level upper-limits for the point-source flux of photons with energies greater than 10^{18}, $10^{18.5}$, 10^{19}, $10^{19.5}$ and 10^{20} eV are 0.094, 0.029, 0.010, 0.0073 and 0.0058 km^{-2} yr^{-1}, respectively. For energies higher than $10^{18.5}$ eV, the photon point-source limits are set for the first time. Numerical results for each given direction in each energy range are provided as a supplement to this paper.

Key words: methods: data analysis – cosmic rays – gamma-rays: general.

1 INTRODUCTION

Ultra-high-energy (UHE) photons are an important tool for studying the high-energy Universe. A plausible source of photons with exa-eV (EeV) energy is provided by UHE cosmic rays (UHECRs) undergoing the Greisen–Zatsepin–Kuzmin process (Greisen 1966; Zatsepin & Kuzmin 1966) or pair production process (Blumenthal 1970) on a cosmic background radiation. In this context, the EeV photons can be a probe of both UHECR mass composition and the distribution of their sources (Gelmini, Kalashev & Semikoz 2008; Hooper, Taylor & Sarkar 2011). At the same time, the possible flux of photons produced by UHE protons in the vicinity of their sources by pion photoproduction or inelastic nuclear collisions would be noticeable only for relatively near sources, as the attenuation length of UHE photons is smaller than that of UHE protons; see, for example, Bhattacharjee & Sigl (2000) for a review. There also exists a class of so-called top-down models of UHECR generation that efficiently produce the UHE photons, for instance by the decay of heavy dark-matter particles (Berezinsky, Kachelriess & Vilenkin 1997; Kuzmin & Rubakov 1998) or by the radiation from cosmic strings (Berezinsky, Blasi & Vilenkin 1998). The search for the UHE photons was shown to be the most sensitive method of indirect detection of heavy dark matter (Kalashev & Kuznetsov 2016, 2017; Kuznetsov 2017; Kachelriess, Kalashev & Kuznetsov 2018; Alcantara, Anchordoqui & Soriano 2019). Another fundamental physics scenario that could be tested with UHE photons (Fairbairn, Rashba & Troitsky 2011) is the photon mixing with axion-like particles (Raffelt & Stodolsky 1988), which could be responsible for the correlation of UHECR events with BL Lac type objects observed by the High Resolution Fly's Eye (HiRes) experiment (Gorbunov et al. 2004; Abbasi et al. 2006). In most of these scenarios, a clustering of photon arrival directions, rather than diffuse distribution, is expected, so point-source searches can be a suitable test for photon - axion-like particle mixing models. Finally, UHE photons could also be used as a probe for the models of Lorentz-invariance violation (Coleman & Glashow 1999; Galaverni & Sigl 2008; Maccione, Liberati & Sigl 2010; Rubtsov, Satunin & Sibiryakov 2012, 2014).

The Telescope Array (TA; Tokuno et al. 2012; Abu-Zayyad et al. 2013c) is the largest cosmic ray experiment in the Northern Hemisphere. It is located at 39.3° N, 112.9° W in Utah, USA. The observatory includes a surface detector array (SD) and 38 fluorescence telescopes grouped into three stations. The SD consists of 507 stations that contain plastic scintillators, each with an area of 3 m² (SD stations). The stations are placed in the square grid with 1.2 km spacing and cover an area of ∼700 km². The TA SD is capable of detecting extensive air showers (EASs) in the atmosphere caused by cosmic particles of EeV and higher energies. The TA SD has been operating since 2008 May.

A hadron-induced EAS significantly differs from an EAS induced by a photon because the depth of the shower maximum X_{max} for a photon shower is larger, and a photon shower contains fewer muons and has a more curved front (see Risse & Homola 2007 for a review). The TA SD stations are sensitive to both muon and electromagnetic components of the shower and therefore can be triggered by both hadron-induced and photon-induced EAS events.

In the present study, we use 9 yr of TA SD data for a blind search for point sources of UHE photons. We utilize the statistics of the SD data, which benefit from a high duty cycle. The full Monte Carlo (MC) simulation of proton-induced and photon-induced EAS events allows us to perform the photon search up to the highest accessible energies, $E \gtrsim 10^{20}$ eV. As the main tool for the present photon search, we use a multivariate analysis based on a number of SD parameters that make it possible to distinguish between photon and hadron primaries.

While searches for diffuse UHE photons were performed by several EAS experiments, including Haverah Park (Ave et al. 2000), AGASA (Shinozaki et al. 2002; Risse et al. 2005), Yakutsk (Rubtsov et al. 2006; Glushkov et al. 2007, 2010), Pierre Auger (Abraham et al. 2007, 2008a; Bleve 2016; Aab et al. 2017c) and TA (Abu-Zayyad et al. 2013b; Abbasi et al. 2019a), the search for point sources of UHE photons has been done only by the Pierre Auger Observatory (Aab et al. 2014, 2017a). The latter searches were based on hybrid data and were limited to the $10^{17.3} < E < 10^{18.5}$ eV energy range. In the present paper, we use the TA SD data alone. We perform the searches in five energy ranges: $E > 10^{18}$, $E > 10^{18.5}$, $E > 10^{19}$, $E > 10^{19.5}$ and $E > 10^{20}$ eV. We find no significant evidence of photon point sources in all energy ranges and we set the point-source flux upper limits from each direction in the TA field of view (FOV). The search for unspecified neutral particles was also previously performed by the TA (Abbasi et al. 2015). The limit on the point-source flux of neutral particles obtained in that work is close to the present photon point-source flux limits.

2 TA SD DATA AND RECONSTRUCTION

2.1 Data set and Monte Carlo simulations

The data set and MC simulations used in this study are the same as in the recent TA search for diffuse photons (Abbasi et al. 2019a). We use the TA SD data set obtained from 9 yr of observations, from 2008 May 11 to 2017 May 10. During this period, the duty cycle of the SD was about 95 per cent (Abu-Zayyad et al. 2013a; Matthews 2018).

The MC simulations used in this study reproduce 9 yr of TA SD observations, as shown in Matthews (2018). We simulate separately showers induced by photon and proton primaries for the signal

and background estimations, respectively,[1] using the CORSIKA code (Heck et al. 1998). The high-energy nuclear interactions are simulated with the QGSJET-II-03 model (Ostapchenko 2006), the low-energy nuclear reactions with the FLUKA package (Ferrari et al. 2005) and the electromagnetic shower component with the EGS4 model (Nelson, Hirayama & Rogers 1985). The use of the PRESHOWER package (Homola et al. 2005), which takes into account the splitting of the UHE photon primaries into the Earth's magnetic field, allows us to correctly simulate photon-induced EASs up to the 100 EeV primary energy and higher. The thinning and dethinnig procedures, with parameters described in Stokes et al. (2012), are used to reduce the calculation time.

We simulated 2100 CORSIKA showers for photon primaries and 9800 for proton primaries in the $10^{17.5}-10^{20.5}$ eV primary energy range. The power spectrum for CORSIKA photon events is set to E^{-1}. The showers from the photon and proton libraries are processed by the code simulating the real-time calibration SD response by means of the GEANT4 package (Agostinelli et al. 2003). Each CORSIKA event is thrown to a random location within the SD area multiple times. For photons, these procedures also include reweighting of the events to the E^{-2} differential spectrum, which is assumed for primary photons in this work. As a result, a set of 57 million photon events with the E^{-2} spectrum was obtained. The proton MC set used in this study contains approximately 210 million events. Details of proton MC simulations are described in Abu-Zayyad et al. (2013a, 2014) and Matthews (2018). The format of the MC events is the same as the one used for real events, so both the data set and MC simulations are processed by one and the same reconstruction procedure (Abu-Zayyad et al. 2014), as described below.

2.2 Reconstruction

In this paper, the same procedure to reconstruct shower parameters is used as in the previous TA photon searches (Abu-Zayyad et al. 2013b; Abbasi et al. 2019a). Each event, real or simulated, is reconstructed by a joint fit of the shower-front geometry and the lateral distribution function (LDF). This allows us to determine the shower parameters, including the arrival direction, the core location, the signal density at the fixed distance from the core and the shower front curvature parameter (see Abu-Zayyad et al. 2013b for details).

We apply the following set of quality cuts for both MC and data events:

(i) zenith angle cut, $0° < \theta < 60°$;
(ii) the number of stations triggered is seven or more;
(iii) the shower core is inside the array boundary with the distance to the boundary larger than 1200 m;
(iv) joint fit quality cut, $\chi^2/$d.o.f. < 5.

We also use an additional cut to eliminate the events induced by lightning. It was previously found by the TA Collaboration that lightning strikes could cause events mimicking EAS events, the so-called terrestrial gamma-ray flashes (TGFs; Abbasi et al. 2017, 2018a). Moreover, as the lightning strikes are expected to be electromagnetic, they resemble photon-induced showers. Therefore, the rejection of these events is crucial for photon searches. To carry out this rejection, we use the Vaisala lightning data base from the

US National Lightning Detection Network[2] (NLDN; Cummins & Murphy 2009; Nag et al. 2011). From this data base, we extract a list of NLDN lightning events detected within a circle of 15-mile radius from the Central Laser Facility of the TA, which contains all the TA SD stations, in the time range from 2008-05-11 to 2017-05-10. The list contains 31 622 events grouped in time in such a way that a total of 910 astronomical hours contain one or more lightning strikes. To clean up all possible lightning-induced events from the data set, we remove all the events that occur within time intervals of 10 min before or after the NLDN lightning events. This cut removes the events known to be related to the TGFs, reducing the total exposure only by 0.66 per cent and the total number of data events by 0.77 per cent.

The basic observables, such as zenith angle, calculated in the reconstruction procedure, together with several additional parameters (see below), are used to distinguish photon and proton events by means of a multivariate analysis. Some of the observables utilize features of the experiment's SD technical design, such as the double-layered scintillators. A detailed description of these technical parameters is given in Abu-Zayyad et al. (2013c). The full list of 16 parameters used in the present photon search is the same as in the TA SD search for diffuse photons (Abbasi et al. 2019a) and the TA SD composition study (Abbasi et al. 2019b). These parameters are the following.

(i) The zenith angle, θ.
(ii) The signal density at 800 m from the shower core, S_{800}.
(iii) The Linsley front curvature parameter, a, obtained from the fit of the shower front with the AGASA-modified Linsley time delay function (Teshima et al. 1986; Abu-Zayyad et al. 2013b).
(iv) The area-over-peak (AoP) of the signal at 1200 m (Abraham et al. 2008b).
(v) The AoP slope parameter (Rubtsov & Troitsky 2015).
(vi) The number of stations with a Level-0 trigger (Abu-Zayyad et al. 2013c) (triggered stations).
(vii) The number of stations excluded from the fit of the shower front due to a large contribution to χ^2.
(viii) $\chi^2/$d.o.f. of the shower front fit.
(ix) *The S_b parameter for $b = 3$, where S_b is defined as the bth moment of the LDF:

$$S_b = \sum_i \left[S_i \times (r_i/r_0)^b \right]. \tag{1}$$

Here, S_i is the signal of the ith station, r_i is the distance from the shower core to a given station, $r_0 = 1000$ m. The sum is calculated over all triggered non-saturated stations. S_b is proposed as a composition-sensitive parameter in Ros et al. (2013).

(x) *The S_b parameter for $b = 4.5$.
(xi) The sum of signals of all triggered stations of the event.
(xii) An average asymmetry of signal at the upper and lower layers of the stations, defined as

$$\mathcal{A} = \frac{\sum_{i,\alpha} |s_{i,\alpha}^{\text{upper}} - s_{i,\alpha}^{\text{lower}}|}{\sum_{i,\alpha} |s_{i,\alpha}^{\text{upper}} + s_{i,\alpha}^{\text{lower}}|}, \tag{2}$$

where $s_{i,\alpha}^{\text{upper|lower}}$ is the FADC value of upper or lower layer of the ith station at the α time bin. The sum is calculated over all triggered non-saturated stations over all time bins of the corresponding FADC traces.

---

[1]We justify the proton background assumption in Section 3.1.

[2]Data base of U.S. National Lightning Detection Network® is provided by Vaisala Inc., see https://www.vaisala.com/en/products/data-subscriptions-a nd-reports/data-sets/nldn

Table 1. Bias in the reconstruction of the zenith angle and angular resolution for the photon primaries at various energies.

E_γ (eV)	$\langle \theta_{\text{rec.}} - \theta_{\text{true}} \rangle$	Ang. resolution
$> 10^{18.0}$	$-2.25°$	$3.00°$
$> 10^{18.5}$	$-2.24°$	$2.92°$
$> 10^{19.0}$	$-2.16°$	$2.64°$
$> 10^{19.5}$	$-2.06°$	$2.21°$
$> 10^{20.0}$	$-1.72°$	$2.06°$

(xiii) The total number of peaks of FADC traces summed over upper and lower layers of all triggered stations of the event. To suppress accidental peaks as a result of FADC noise, we define a peak as a time bin with a signal above 0.2 vertical equivalent muons (VEMs), which is higher than the signal of the three preceding and three consequent time bins.

(xiv) The number of peaks for the station with the largest signal.

(xv) The total number of peaks present in the upper layer and not in the lower layer, summed over all triggered stations of the event.

(xvi) The total number of peaks present in the lower layer and not in the upper layer, summed over all triggered stations of the event.

For each MC and data event, we also define the 'photon energy' parameter E_γ, which is the expected energy of the primary particle assuming it is a photon. This energy parameter is calculated as the function of the zenith angle and the S_{800} parameter from the photon MC simulations (Abu-Zayyad et al. 2013b). For proton MC events, as well as for the majority of data events, the E_γ parameter is not the actual primary energy but merely a parameter needed for the consistent comparison of proton events and possible photon events. It is important to note that for the majority of proton-induced events, the reconstructed E_γ parameter is systematically higher than that of photon-induced events of the same primary MC energy. For instance, at ~ 10 EeV MC energy, the mean E_γ for protons is ~ 40 per cent higher than that for photons, if we assume the averaging over the zenith angle. Thus, the proton background for the SD photon search is higher with respect to the hypothetical ideal situation when the energy reconstruction bias is independent of the primary particle type. All the energy values considered in this work are assumed to be E_γ values, unless the other meaning is specified.

The reconstructed values of shower zenith angle, θ_{rec}, for photon primaries are systematically underestimated. The possible reason for this is the azimuthal asymmetry of the shower front, which originates from the fact that, when it arrives, the shower is younger at the front-side stations and older at the back-side stations. The reconstruction bias is defined as a deviation of the event θ_{rec} from a real MC zenith angle of this event, θ_{true}. The average values of this bias for various energies E_γ are given in Table 1. In this study, we correct both proton and photon MC events and data events by these average bias values. This correction allows us to restore the arrival directions of possible photon-induced events more accurately, while not affecting the background of hadron-induced events, which is known to be highly isotropic (Deligny, Kawata & Tinyakov 2017). Another crucial parameter for the point-source search is the angular resolution of the experiment. It is defined as a 0.68 percentile of a distribution of MC events over the opening angle between the event reconstructed arrival direction and the real MC arrival direction. The angular resolution of TA SD for proton primaries at proton energy, $E_p = 10^{19}$ eV, was estimated to be $1.5°$ (Abu-Zayyad et al. 2012). As mentioned above, in the present study we use the reconstruction of Abu-Zayyad et al. (2013b) for both data and MC events. Using

the photon MC set, after applying the zenith-angle bias correction described above, we estimate the angular resolution for photon primaries at various energies E_γ. The results are shown in Table 1.

3 ANALYSIS.

3.1 Multivariate analysis

The analysis method used in this study to distinguish between photon and proton events is a boosted decision tree (BDT) classifier built with the 16 observable parameters listed in the previous section. As an implementation of this method, we use the AdaBoost algorithm (Freund & Schapire 1997) from the TMVA package (Hocker et al. 2007) for ROOT (Brun & Rademakers 1997), in the same way as in the recent TA studies (Abbasi et al. 2019a, b).

The BDT is trained to separate proton MC events from photon MC events. Both proton and photon MC sets are split into three parts with an equal amount of events in each: one for training the classifier, a second one for testing the classifier and the last one for the calculation of proton background and photon effective exposure. We train the classifier separately in five photon energy ranges: $E_\gamma > 10^{18}$ eV, $E_\gamma > 10^{18.5}$ eV, $E_\gamma > 10^{19}$ eV, $E_\gamma > 10^{19.5}$ eV and $E_\gamma > 10^{20}$ eV. As a result of the BDT procedure, the single multivariate analysis (MVA) parameter ξ is assigned to each MC and data event. ξ is defined to take values in the range $-1 < \xi < 1$, where proton-induced events tend to have negative ξ values, and photon-induced events tend to have positive ξ values. The resulting ξ distributions of the MC events from the testing sets and the data events for all considered energy ranges are shown in Fig. 1.

From Fig. 1, which shows the distributions of data and MC events irrespective of the direction in the sky, we can see no deviation from the proton distribution in the expected photon signal region. However, possible excesses in one or several separate directions in the sky could be overlooked if we analyse the all-sky averaged ξ distribution. Hereafter, we discuss the method to set the photon-flux upper limit and to search for photon excesses from separate directions on the sky, and we present respective results.

It is important to note that at primary energies of the order of EeV and higher there is a potential systematic uncertainty in the estimation of the hadron background for the photon signal. The bulk of the events are induced by protons and/or nuclei, but their mass composition is not known precisely (Aab et al. 2017b; Abbasi et al. 2018b, 2019b). We have examined ξ distributions of the iron nucleus-induced events and we have found that, on average, the iron-induced events are less photon-like than proton-induced events. The results of TA work (Abbasi et al. 2019b), where the similar BDT classifier was used, implies that a mixed nuclei ξ distribution would also deviate from the photon ξ distribution more strongly than the proton ξ distribution. Therefore, the assumption of the proton background for the photon search is conservative. However, we also perform an independent photon search, assuming a more realistic mixed nuclei background inferred from the TA SD data in our study (Abbasi et al. 2019b).

3.2 Photon-flux upper limit

In general, the flux upper limit for the particular type of primaries is defined as

$$F_{\text{UL}} = \frac{\mu_{\text{FC}}(N_{\text{obs}}, N_{\text{bg}})}{A_{\text{eff}}}, \quad (3)$$
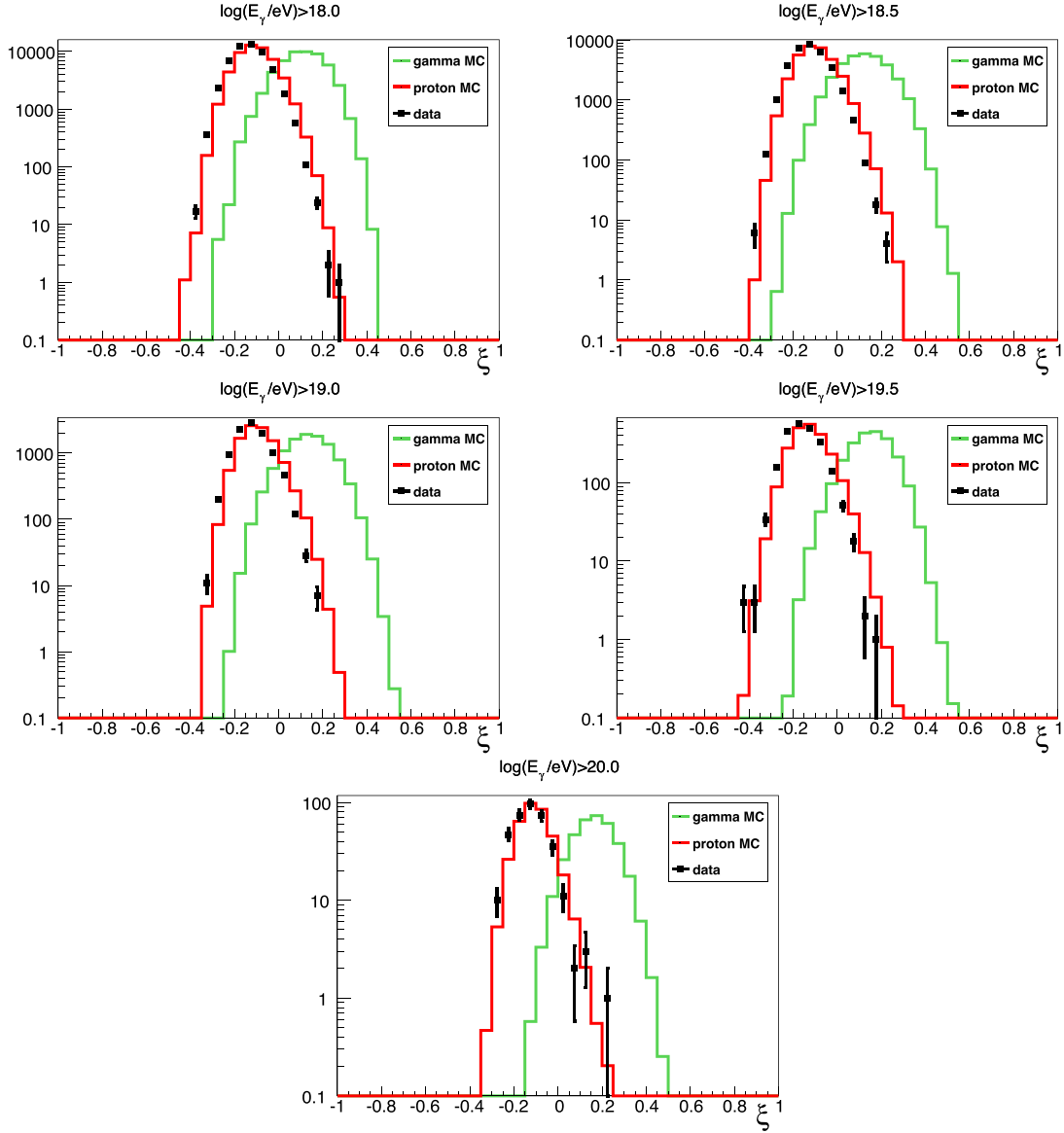
Figure 1. Distributions of the photon and proton MC and data events over the ξ parameter for the five energy ranges (solid red, protons; solid green, photons; black dots, data).

where N_{obs} is the number of detected events of a given type in a given energy range, N_{bg} is the estimated number of background events in the same energy range, μ_{FC} is the upper bound of the respective Poisson mean for the given confidence level (CL), defined according to Feldman & Cousins (1998), and A_{eff} is the effective exposure of the experiment for the given type of primaries in the same energy range.

In the present upper-limit calculation, we assume the null hypothesis (i.e. there are actually no photons and any excess counts from the expected background, $N_{obs} - N_{bg}$, are considered as a fluctuation of the background).

We consider two options of the background estimation. First, $N_{bg} = 0$, an assumption that is conservative because, for fixed N_{obs}, the upper-limit value is higher for a lower value of N_{bg}. Second, we consider a 'real' background of mixed nuclei with the mean $\ln A$ following the one derived from the same TA SD data with the same MVA method in our work (Abbasi et al.

2019b). This background is estimated by down-scaling of the proton background to the respective mean $\ln A$, linearly with $\ln A$, taking into account the recaling of the SD energy scale used in Abbasi et al. (2019b) to the E_γ energy scale used in this work.

The separation between photon and proton primaries is defined by a cut on the MVA variable ξ. The cut is set at some value ξ_0 so that any proton with $\xi > \xi_0$ is considered as a photon candidate and any photon with $\xi > \xi_0$ is contributing to the effective exposure.

To find the minimum value of F_{UL}^γ as a function of ξ_0, we optimize the cut position assuming $N_{obs} = N_p(\xi > \xi_0)$, where $N_p(\xi > \xi_0)$ is the number of protons passing the ξ-cut. As we can see from Fig. 1, the number of MC photon events passing the ξ-cut is decreasing with the growth of ξ_0, leading to a respective decrease of the exposure A_{eff}^γ. Also, the number of photon candidates, $N_{obs} = N_p(\xi > \xi_0)$, is decreasing, but $N_{obs} = 0$ yields a constant non-zero value of μ_{FC}.

This implies that there indeed should be a non-trivial minimum value of F_{UL}^{γ} as a function of ξ_0.

For the ξ-cut optimization, we use the proton MC set, normalized to the size of the data set, and the photon MC set, which is used for the calculation of the photon effective exposure A_{eff}^{γ}. It is important to note that the optimization procedure tends to place ξ_0 at the right edge of the proton distribution in Fig. 1, so the number of candidates N_{obs} and the upper-limit value F_{UL} are subject to fluctuations. These fluctuations become apparent when we consider upper limits for particular directions in the sky with a small number of events.

Until now, the procedures for the upper-limit calculation and cut optimization were similar to those used to search for diffuse photons (Abbasi et al. 2019a). The difference of the analysis procedure used here from that of Abbasi et al. (2019a) is in the use of the separate event sets for different directions in the sky. The ξ-cut is also optimized separately for every direction studied. We pixellize the sky in equatorial coordinates $\{\alpha, \delta\}$ using the HEALPix package (Gorski et al. 2005) into 12 288 pixels ($N_{side} = 32$). For the pixel i with the centre $\{\alpha_i, \delta_i\}$, the corresponding data set contains events located inside a spherical cap region around the pixel centre within an angular distance that equals the experiment's angular resolution at the respective energy (see Table 1).[3]

The effective exposure of the experiment to photons at the pixel i is given by

$$A_{eff}^i = S\,T\,\overline{\cos\theta_i}\,\frac{N_{MC,\gamma}^i(\xi > \xi_0)}{N_{MC,\gamma}^i}, \tag{4}$$

where S is the area of the experiment, T is the period of observation, θ_i is the zenith angle at which the pixel i is seen by the experiment, $N_{MC,\gamma}^i$ is the total number of photon events simulated in the respective pixel and $N_{MC,\gamma}^i(\xi > \xi_0)$ is the number of these events that pass the ξ-cut. The same pixel in equatorial coordinates is seen by the experiment at different θ depending on time, so the diurnal mean value $\overline{\cos\theta}$ is used. It is given by the expression (Sommers 2001)

$$\overline{\cos\theta} = \cos\lambda_0\,\cos\delta\,\sin\alpha_m + \alpha_m\,\sin\lambda_0\,\sin\delta, \tag{5}$$

where δ is the declination, λ_0 is the geographical latitude of the experiment, θ_{max} is the maximum zenith angle of the events considered in the particular analysis and α_m is given by the expression

$$\alpha_m = \begin{cases} 0; & \zeta > 1 \\ \pi; & \zeta < -1 \\ \arccos\zeta; & -1 < \zeta < 1 \end{cases}, \tag{6}$$

where

$$\zeta = \frac{(\cos\theta_{max} - \sin\lambda_0\,\sin\delta)}{\cos\lambda_0\,\cos\delta}. \tag{7}$$

The 'effective' part of the exposure, $[N_{MC,\gamma}^i(\xi > \xi_0)]/N_{MC,\gamma}^i$, is calculated using the photon MC set. To have enough statistics for this calculation, we need to generate separate MC sets for each sky-map pixel. However, this is technically unreasonable, as the exposure depends only on the declination of the given pixel. We use the following method to increase the MC statistics in each pixel:

ξ_0 is optimized over the events belonging to the whole constant-declination band, whose width is twice the angular resolution centred in the given pixel. This method resembles the so-called scrambling technique (Cassiday et al. 1990), which was used, for instance, in the Pierre Auger Observatory search for photon point sources (Aab et al. 2014). The additional advantage of the method used is the preservation of relatively large effective statistics of the MC events in each pixel, including the variety over the ξ parameter. We have found that, in this case, fluctuations of the ξ_0 position between adjacent pixels are smaller, compared with the standard scrambling technique. It is reasonable to smooth these fluctuations even further by making a least-squares fit of a ξ_0 position as a function of declination with a smooth function, for which we use a second-order polynomial. As mentioned before, the flux upper limit remains conservative after this operation. The examples of ξ_0 as a function of declination and its smooth fitting are shown in Fig. 2.[4]

As the ξ_0 position for the pixel i is fixed, the actual upper-limit value is calculated using the definition (3) with $N_{obs}^i = N_{data}^i(\xi > \xi_0)$, where N_{data}^i is the number of data events belonging to the respective pixel and $N_{bg}^i = 0$ or $N_{bg}^i = N_{\ln A}^i(\xi > \xi_0)$, where $N_{\ln A}^i$ is the number of real background events.

The TA FOV for the considered zenith angle cut ($0° < \theta < 60°$) spans from $-20.7°$ to $90°$ in declination. However, the event statistics is low in the constant-declination bands near the edges of this interval. Therefore, we reduce the considered sky region to $-15.7° \leq \delta \leq 85°$. It contains 7848 pixels.

3.3 Results

Fig. 3 shows the 95 per cent CL photon-flux upper limits calculated with a zero background assumption for each pixel in the TA FOV and for various photon energies. The numerical values of these limits as well as the limits calculated with the "real" background assumption are given in the supporting information. The values of the limits averaged over all pixels are presented in Table 2.

The null hypothesis assumed for the photon upper-limit calculation is not optimal for the photon search. However, a rough estimation of the possible photon signal can be made in this set-up. We optimize ξ_0 in each declination band with the same assumptions as in the previous section, and we estimate the background in each pixel as the appropriately normalized number of protons that pass the cut: $N_{MC,p}^i(\xi > \xi_0)$. For the calculation of photon excess, the assumption of a proton background is conservative, because it should be higher than any mixed nuclei background, as discussed in Section 3.1. The background maps for various photon energies are shown in Fig. 4. The maxima over all pixels of the pre-trial photon candidate excesses over the proton background are presented in Table 2, along with the average values of the proton background. The highest pre-trial excess significance, 3.43σ ($N_{bg} = 0.036$ and $N_{obs} = 2$), appears in the highest energy bin $E_{\gamma} > 10^{20}$ eV, at $\{\alpha = 155.3°, \delta = 60.4°\}$ pixel. To make a simple estimation of the post-trial p-value, we can use the Bonferroni correction, which is to multiply the number of trials by the mimimum pre-trial excess p-value (Miller 1981). In turn, the number of trials could be estimated as the number of non-overlapping pixel-sized regions of the map, which is several times smaller than the actual number of pixels. The resulting post-trial significances estimated in this way appear

---

[3]The distance between any pixel centres is smaller than the experiment's angular resolution at all considered energies, so the experiment's FOV is overlapped without gaps, but some events in adjacent pixels could be the same.

[4]The ξ_0 points for adjacent declination bands are clustered because these bands are overlapping with each other and a part of their MC events is one and the same.
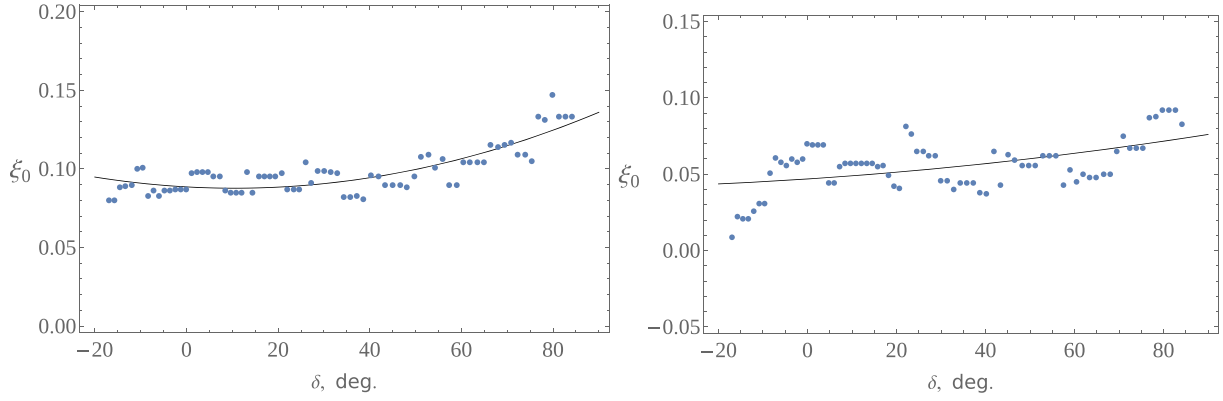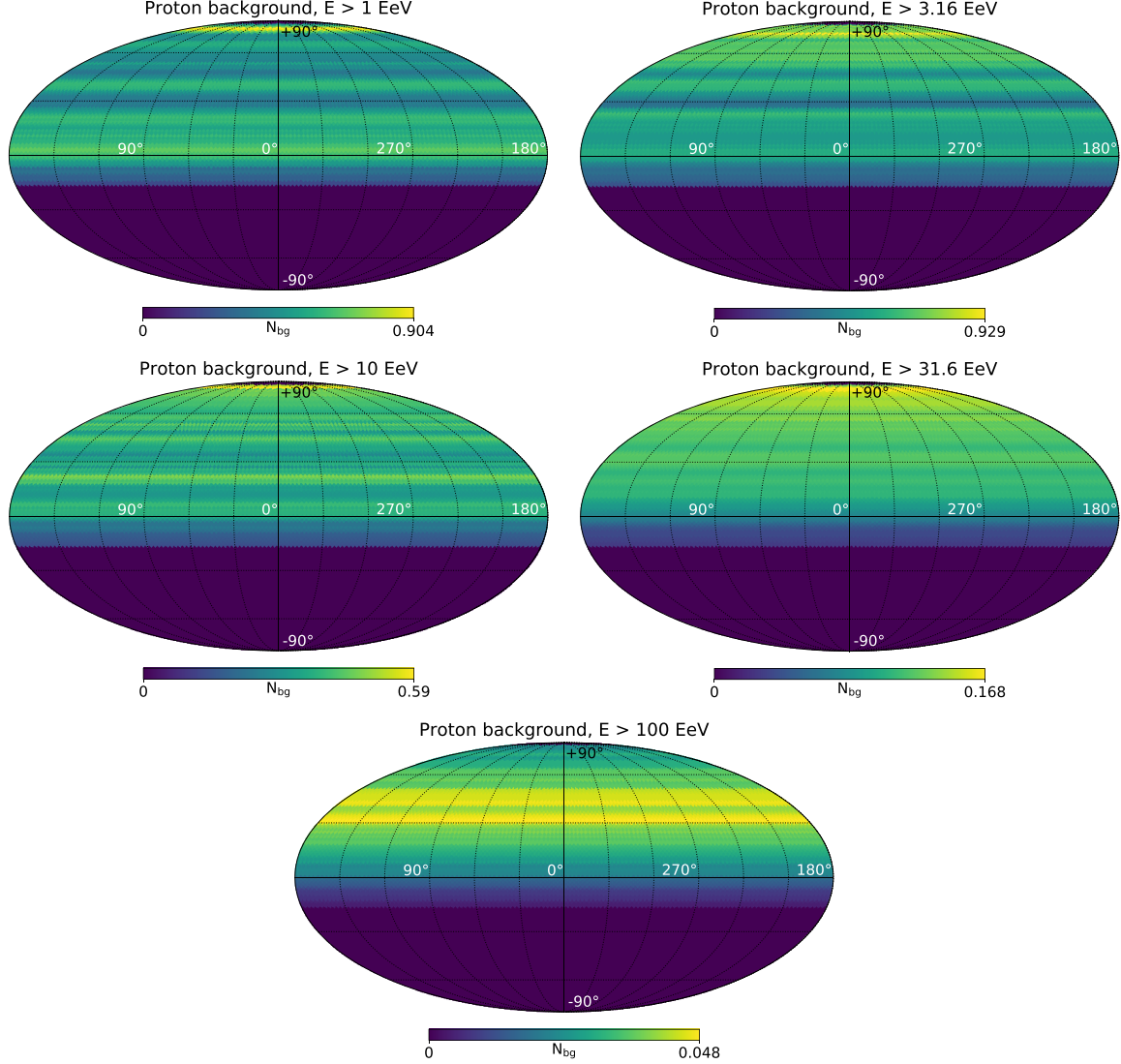
Figure 2. Examples of ξ_0 position as a function of declination and its smooth fitting for $E_\gamma > 10^{18}$ eV (left panel) and $E_\gamma > 10^{19}$ eV (right panel) photons. Blue points are the cut positions obtained with the optimization of the photon-flux upper limit (equation 3) in the respective declination bands.
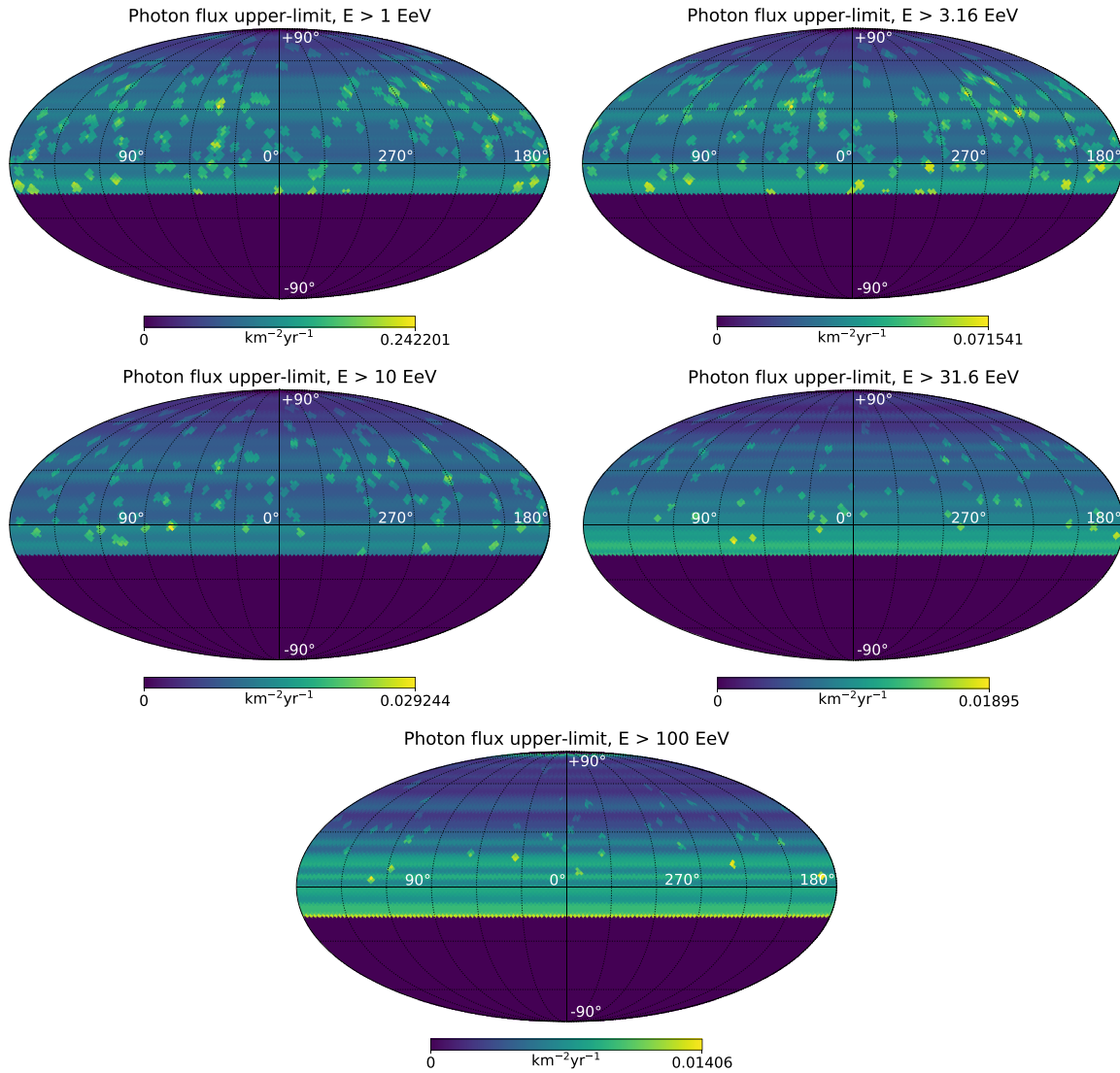
Figure 3. Maps of point-source photon-flux upper limits (95 per cent CL) for various photon energies calculated with a zero background assumption and plotted in equatorial coordinates.

Table 2. Point-source photon-flux upper limits and proton backgrounds averaged over all pixels together with the maximum pre-trial significance of the photon excess over the proton background.

E_γ (eV)	$\langle F_\gamma \rangle \leq$ (km^{-2} yr^{-1}; zero bg.)	$\langle F_\gamma \rangle \leq$ (km^{-2} yr^{-1}; "real" bg.)	$\langle N_{bg} \rangle$	max. γ signif. (pre-trial)
$>10^{18.0}$	0.094	0.069	0.49	2.72 σ
$>10^{18.5}$	0.029	0.021	0.52	2.71 σ
$>10^{19.0}$	0.010	0.0074	0.34	2.89 σ
$>10^{19.5}$	0.0071	0.0055	0.10	2.76 σ
$>10^{20.0}$	0.0058	0.0045	0.029	3.43 σ

Figure 4. Distributions of the numbers of proton background events over the sky map for the various photon energies, plotted in equatorial coordinates.

to be below the 1σ level for all points of the sky at all considered energies. Therefore, we conclude that, at the present level of point-source photon search sensitivity, there is no evidence for the photon signal. The actual results for each sky-map pixel at various energies are given in the text files supplementary to this paper. The format of the files is described in the Supporting Information.

The main systematic uncertainties for the photon-flux upper limits are related to the overestimation of the E_γ parameter for hadron-induced events and to the uncertainty of the primary hadron mass composition. The former uncertainty leads to the overestimation of

the hadron background and subsequently to the looser photon-flux upper limit. As for the uncertainty in hadron mass composition, the assumption of the proton composition, which we used for the ξ-cut optimization, could only make the photon-flux upper limit looser compared with a mixed nuclei composition case. Therefore, the limits set are conservative with respect to both of these uncertainties.

Finally, the last assumption that affects the result is the assumption of the background in equation (3). The most conservative limits are set for a zero background assumption, while the "real" mixed nuclei background assumption yields more realistic limits.

4 DISCUSSION AND CONCLUSIONS

The upper limits are set on the fluxes of photons from each particular direction in the sky in the TA FOV, according to the experiment's angular resolution with respect to photons. So far, the only results of the UHE point-source photon-flux upper limits presented are those by the Pierre Auger experiment (Aab et al. 2014, 2017a). The comparison of those results with ours is not straightforward as the photon energy range of the Auger search, $10^{17.3} < E_\gamma < 10^{18.5}$ eV, does not fully coincide with any of our ranges of search. Regardless, the average point-source photon-flux upper limit of Auger, $\langle F_\gamma \rangle \leq 0.035$ km^{-2} yr^{-1}, is two to three times lower than our average limit for $E_\gamma > 10^{18}$ eV. The results for energies larger than $E > 10^{18.5}$ eV are obtained here for the first time.

The point-source photon-flux upper limits derived in the present study can be used to constrain various models of astrophysics and particle physics. We can assume a distribution of photon sources and impose the constraints on their properties using the combination of point-source limits. In principle, these constraints could be stronger than those derived from the diffuse photon-flux limits. The models that could be probed with the present photon point-source flux limits include cosmogenic photon generation models as well as top-down models of UHE photon production, such as heavy decaying dark matter.

REFERENCES

Aab A. et al., 2014, ApJ, 789, 160
Aab A. et al., 2017a, ApJ, 837, L25
Aab A. et al., 2017b, Phys. Rev., D96, 122003
Aab A. et al., 2017c, JCAP, 1704, 009
Abbasi R. U. et al., 2006, ApJ, 636, 680
Abbasi R. U. et al., 2015, ApJ, 804, 133
Abbasi R. et al., 2017, Phys. Lett. A, 381, 2565
Abbasi R. et al., 2018a, J. Geophys. Res. Atmos., 123, 6864
Abbasi R. U. et al., 2018b, ApJ, 858, 76
Abbasi R. U. et al., 2019a, Astropart. Phys., 110, 8
Abbasi R. U. et al., 2019b, Phys. Rev., D99, 022002
Abraham J. et al., 2007, Astropart. Phys., 27, 155
Abraham J. et al., 2008a, Astropart. Phys., 29, 243
Abraham J. et al., 2008b, Phys. Rev. Lett., 100, 211101
Abu-Zayyad T. et al., 2012, ApJ, 757, 26
Abu-Zayyad T. et al., 2013a, ApJ, 768, L1
Abu-Zayyad T. et al., 2013b, Phys. Rev., D88, 112005
Abu-Zayyad T. et al., 2013c, Nucl. Instrum. Meth., A689, 87
Abu-Zayyad T. et al., 2014, preprint (arXiv:1403.0644)
Agostinelli S. et al., 2003, Nucl. Instrum. Meth., A506, 250
Alcantara E., Anchordoqui L. A., Soriano J. F., 2019, preprint (arXiv:1903.05429)
Ave M., Hinton J. A., Vazquez R. A., Watson A. A., Zas E., 2000, Phys. Rev. Lett., 85, 2244
Berezinsky V., Kachelriess M., Vilenkin A., 1997, Phys. Rev. Lett., 79, 4302
Berezinsky V., Blasi P., Vilenkin A., 1998, Phys. Rev., D58, 103515
Bhattacharjee P., Sigl G., 2000, Phys. Rept., 327, 109
Bleve C., 2016, PoS, ICRC2015, 1103
Blumenthal G. R., 1970, Phys. Rev., D1, 1596
Brun R., Rademakers F., 1997, Nucl. Instrum. Meth., A389, 81
Cassiday G. L. et al., 1990, Nucl. Phys. Proc. Suppl., 14A, 291
Coleman S. R., Glashow S. L., 1999, Phys. Rev., D59, 116008
Cummins K., Murphy M. J., 2009, IEEE Trans., 51, 499
Deligny O., Kawata K., Tinyakov P., 2017, PTEP, 2017, 12A104
Fairbairn M., Rashba T., Troitsky S. V., 2011, Phys. Rev., D84, 125019
Feldman G. J., Cousins R. D., 1998, Phys. Rev., D57, 3873
Ferrari A., Sala P. R., Fasso A., Ranft J., 2005, CERN–2005-010
Freund Y., Schapire R., 1997, Journal of Computer and System Sciences, 55, 119,
Galaverni M., Sigl G., 2008, Phys. Rev. Lett., 100, 021102
Gelmini G., Kalashev O. E., Semikoz D. V., 2008, J. Exp. Theor. Phys., 106, 1061
Glushkov A. V., Gorbunov D. S., Makarov I. T., Pravdin M. I., Rubtsov G. I., Sleptsov I. E., Troitsky S. V., 2007, JETP Lett., 85, 131
Glushkov A. V., Makarov I. T., Pravdin M. I., Sleptsov I. E., Gorbunov D. S., Rubtsov G. I., Troitsky S. V., 2010, Phys. Rev., D82, 041101
Gorbunov D. S., Tinyakov P. G., Tkachev I. I., Troitsky S. V., 2004, JETP Lett., 80, 145
Gorski K. M., Hivon E., Banday A. J., Wandelt B. D., Hansen F. K., Reinecke M., Bartelman M., 2005, ApJ, 622, 759
Greisen K., 1966, Phys. Rev. Lett., 16, 748
Heck D., Knapp J., Capdevielle J. N., Schatz G., Thouw T., 1998, CORSIKA: A Monte Carlo Code to Simulate Extensive Air Showers, FZKA-6019. Forschungszentrum Karlsruhe GmbH, Karlsruhe
Hocker A. et al., 2007, PoS, ACAT, 040
Homola P., Gora D., Heck D., Klages H., Pekala J., Risse M., Wilczynska B., Wilczynski H., 2005, Comput. Phys. Commun., 173, 71
Hooper D., Taylor A. M., Sarkar S., 2011, Astropart. Phys., 34, 340
Kachelriess M., Kalashev O. E., Kuznetsov M. Yu., 2018, Phys. Rev., D98, 083016

Kalashev O. E., Kuznetsov M. Yu., 2016, Phys. Rev., D94, 063535
Kalashev O. E., Kuznetsov M. Y., 2017, JETP Lett., 106, 73
Kuzmin V. A., Rubakov V. A., 1998, Phys. Atom. Nucl., 61, 1028
Kuznetsov M. Yu., 2017, JETP Lett., 105, 561
Maccione L., Liberati S., Sigl G., 2010, Phys. Rev. Lett., 105, 021101
Matthews J., 2018, PoS, ICRC2017, 1096
Miller R. G. J., 1981, Simultaneous Statistical Inference. Springer, New York
Nag A. et al., 2011, J. Geophys. Res., 116, D02123
Nelson W. R., Hirayama H., Rogers D. W. O., 1985, preprint (SLAC–0265)
Ostapchenko S., 2006, Nucl. Phys. Proc. Suppl., 151, 143
Raffelt G., Stodolsky L., 1988, Phys. Rev., D37, 1237
Risse M., Homola P., 2007, Mod. Phys. Lett., A22, 749
Risse M., Homola P., Engel R., Gora D., Heck D., Pekala J., Wilczynska B., Wilczynski H., 2005, Phys. Rev. Lett., 95, 171102
Ros G., Supanitsky A. D., Medina-Tanco G. A., del Peral L., Rodrguez-Fras M. D., 2013, Astropart. Phys., 47, 10
Rubtsov G. I., Troitsky S. V., 2015, J. Phys. Conf. Ser., 608, 012067
Rubtsov G. I. et al., 2006, Phys. Rev., D73, 063009
Rubtsov G., Satunin P., Sibiryakov S., 2012, Phys. Rev., D86, 085012
Rubtsov G., Satunin P., Sibiryakov S., 2014, Phys. Rev., D89, 123011
Shinozaki K. et al., 2002, ApJ, 571, L117
Sommers P., 2001, Astropart. Phys., 14, 271
Stokes B. T., Cady R., Ivanov D., Matthews J. N., Thomson G. B., 2012, Astropart. Phys., 35, 759
Teshima M. et al., 1986, J. Phys. G, 12, 1097
Tokuno H. et al., 2012, Nucl. Instrum. Meth., A676, 54
Zatsepin G. T., Kuzmin V. A., 1966, JETP Lett., 4, 78

SUPPORTING INFORMATION

Supplementary data are available at *MNRAS* online.

Photon point-source flux upper limits and photon excess pre-trial significances for all sky-map pixels are summarized in a separate file for each energy bin, called limit_[log (E_γ/eV)].txt. The file contains several columns with the following data:

Column 1, HEALPix pixel number (RING, started from 24);
Column 2, pixel α, rad;
Column 3, pixel δ, rad;
Column 4, ξ-cut value;
Column 5, proton background value;
Column 6, number of γ-candidate events;
Column 7, 95 per cent CL F_γ upper limit, km^{-2} yr^{-1} (zero background assumption);
Column 8, 95 per cent CL F_γ upper limit, km^{-2} yr^{-1} ("real" background assumption);
Column 9, pre-trial γ excess p-value;
Column 10, pre-trial γ excess significance.

As mentioned in Section 3.3, the proton background value is used only for the calculation of the photon excess p-value and significance, while the upper limits are calculated with either a zero background assumption or a "real" mixed nuclei background assumption. For pixels with the number of γ-candidates less than p background, both p-value and significance are set to zero.

Please note: Oxford University Press is not responsible for the content or functionality of any supporting materials supplied by the authors. Any queries (other than missing material) should be directed to the corresponding author for the article.

[1]*High Energy Astrophysics Institute and Department of Physics and Astronomy, University of Utah, Salt Lake City, Utah, USA*

[2]*The Graduate School of Science and Engineering, Saitama University, Saitama, Saitama, Japan*

[3]*Graduate School of Science and Engineering, Tokyo Institute of Technology, Meguro, Tokyo, Japan*

[4]*Department of Physics and The Research Institute of Natural Science, Hanyang University, Seongdong-gu, Seoul, Korea*

[5]*Department of Physics, Tokyo University of Science, Noda, Chiba, Japan*

[6]*Department of Physics, Kindai University, Higashi Osaka, Osaka, Japan*

[7]*Service de Physique Theorique, Universite Libre de Bruxelles, Brussels, Belgium*

[8]*Hakubi Center for Advanced Research, Kyoto University, Sakyo-ku, Kyoto, Japan*

[9]*Graduate School of Science, Kyoto University, Sakyo-ku, Kyoto, Japan*

[10]*Graduate School of Science, Osaka City University, Osaka, Osaka, Japan*

[11]*Institute for Cosmic Ray Research, University of Tokyo, Kashiwa, Chiba, Japan*

[12]*Kavli Institute for the Physics and Mathematics of the Universe (WPI), Todai Institutes for Advanced Study, University of Tokyo, Kashiwa, Chiba, Japan*

[13]*Information Engineering Graduate School of Science and Technology, Shinshu University, Nagano, Nagano, Japan*

[14]*Faculty of Engineering, Kanagawa University, Yokohama, Kanagawa, Japan*

[15]*Interdisciplinary Graduate School of Medicine and Engineering, University of Yamanashi, Kofu, Yamanashi, Japan*

[16]*Astrophysical big bang Laboratory, RIKEN, Wako, Saitama, Japan*

[17]*Department of Physics, Sungkyunkwan University, Jang-an-gu, Suwon, Korea*

[18]*Department of Physics, Tokyo City University, Setagaya-ku, Tokyo, Japan*

[19]*Institute for Nuclear Research of the Russian Academy of Sciences, Moscow, Russia*

[20]*Advanced Research Institute for Science and Engineering, Waseda University, Shinjuku-ku, Tokyo, Japan*

[21]*Department of Physics, Chiba University, Chiba, Chiba, Japan*

[22]*Department of Physics, School of Natural Sciences, Ulsan National Institute of Science and Technology, UNIST-gil, Ulsan, Korea*

[23]*Department of Physics, Yonsei University, Seodaemun-gu, Seoul, Korea*

[24]*Academic Assembly School of Science and Technology Institute of Engineering, Shinshu University, Nagano, Nagano, Japan*

[25]*Faculty of Science, Kochi University, Kochi, Kochi, Japan*

[26]*Nambu Yoichiro Institute of Theoretical and Experimental Physics, Osaka City University, Osaka, Osaka, Japan*

[27]*Department of Physical Sciences, Ritsumeikan University, Kusatsu, Shiga, Japan*

[28]*Sternberg Astronomical Institute, Moscow M.V. Lomonosov State University, Moscow, Russia*

[29]*Department of Physics and Astronomy, Rutgers University - The State University of New Jersey, Piscataway, New Jersey, USA*

[30]*Earthquake Research Institute, University of Tokyo, Bunkyo-ku, Tokyo, Japan*

[31]*Department of Engineering Science, Faculty of Engineering, Osaka Electro-Communication University, Neyagawa-shi, Osaka, Japan*

[32]*Graduate School of Information Sciences, Hiroshima City University, Hiroshima, Hiroshima, Japan*

[33]*Institute of Particle and Nuclear Studies, KEK, Tsukuba, Ibaraki, Japan*

[34]*National Institute of Radiological Science, Chiba, Chiba, Japan*

[35]*CEICO, Institute of Physics, Czech Academy of Sciences, Prague, Czech Republic*

[36]*Department of Physics and Institute for the Early Universe, Ewha Womans University, Seodaaemun-gu, Seoul, Korea*

[37]*Department of Physics, Ehime University, Matsuyama, Ehime, Japan*

This paper has been typeset from a TeX/LaTeX file prepared by the author.